


Collimating Cylindrical Surface Leaky Waves for Highly Improved Radiation Characteristics of Holograms

Mohammad Moein Moeini,^{*} Homayoon Oraizi, and Amrollah Amini

Department of Electrical Engineering, Iran University of Science and Technology, 1684613114 Tehran, Iran

 (Received 16 November 2018; revised manuscript received 10 January 2019; published 2 April 2019)

High-resolution microwave leaky-wave holograms excited by a center-fed cylindrical-surface-wave launcher show a null in the object-wave direction, which is an undesired effect for electromagnetic beamforming. Also, planar leaky-wave metasurfaces generating a tilted beam suffer greatly from the destructive effect of nonforward surface leaky waves at frequencies other than the design frequency and they are operable at almost only a single frequency. Here we propose a two-dimensional modified-hologram configuration using a parabolic surface reflector to collimate the nonforward leaky modes into forward leaky modes. The modified hologram exhibits a null-free radiation pattern and greatly increased operating-frequency bandwidth. The consequent frequency bandwidth provides the scannability property by frequency variation. The forward-mode-dominant surface-wave excitation of the hologram allows the metasurface to generate the object beam more precisely; therefore, high directivity over the operating bandwidth is obtained. The concept is verified by fabrication and experimentally tested, confirming beam maintenance over a reasonable frequency range and scannability property. The measurement results are in excellent agreement with full-wave simulation, prove applicable wideband leaky-wave holograms.

DOI: [10.1103/PhysRevApplied.11.044006](https://doi.org/10.1103/PhysRevApplied.11.044006)

I. INTRODUCTION

Controlling an electromagnetic wave and making it radiate in a desired manner have always attracted tremendous attention in applied electromagnetics; the advent of metamaterials and metasurfaces [1,2] was a breakthrough in radiation engineering. Design and engineering of modulated metamaterials to control a scattered [3] or leaky [4,5] electromagnetic wave have attracted attention in recent literature [6–8]. An electromagnetic wave can be manipulated through metasurfaces to obtain certain properties. Conversion of different wave profiles (e.g. space wave and surface wave) is one of these properties [9,10]. Introduction of leaky waves in electromagnetics has great importance for beam engineering [11]. Leaky-wave systems have wide applications from microwave to optical frequencies [12,13]. Power-leakage engineering using metasurfaces based on variables dependent on the interaction of power generated by a surface-wave launcher and the metasurface is an amazing solution to modern beamforming requirements such as frequency-modulated continuous-wave systems. Gabor [14] firstly introduced the theory of holography in optics in 1948. Holography was restricted to the optical spectrum for many years until Checcacci *et al.* [15] proposed the holographic principle for antenna design and microwave-regime applicability of the theory in 1968. In a sinusoidally modulated surface where the

modulation process is governed by the holographic principle, precise knowledge of the surface impedance on the holographic surface yields exact electromagnetic fields above the surface. A waveguide with a partially reflective interface made of periodic perturbations allows the horizontally guided wave penetrate the interface to form the object wave [16,17]. As the wave travels longer in the waveguide, the object wave built from gradual wave leakage becomes more accurate. The concept of holographic leakage engineering to obtain a desired object wave was proved by Fong *et al.* [5]. On two-dimensional (2D) holographic metasurfaces that are designed to generate a tilted object wave, a cylindrical-surface-wave launcher can be used to excite the modulated surface impedance. Metallic patches can realize the required surface impedance for holographic beamforming by applying the modulation on patch dimensions. The hexagonal metallic patch unit cell can be chosen as an isotropic unit cell to realize the surface impedance.

For a center-fed leaky-wave hologram, while the surface impedance is realized with low resolution, object-wave construction is possible. However, when the holographic surface impedance is realized with high resolution, the radiation pattern tends to approach zero value in the direction of the object wave. This is proved in the next section.

A surface wave that has opposite horizontal wave-number vector relative to the desired leaky wave is

^{*}mohammad_moeini@elec.iust.ac.ir

classified as a backward surface wave [16–18]. The wave leakage corresponding to the backward surface wave in a leaky-wave system deviates from the wave leakage from the forward surface wave when the operating frequency deviates from the design frequency [19,20]. Therefore, holographic leaky-wave systems are capable of beamforming in a narrow vicinity around the design frequency [21,22]. Center-fed modulated surfaces have always suffered from single-frequency operation [5]. In the work reported in Ref. [19], a side-fed hologram was used to try to overcome this problem; however, induced current on the edges around the surface-wave launcher has a destructive effect on the generated object wave. Rearranging a cylindrical surface leaky wave in a way that the forward surface wave participates more than the nonforward surface wave in object wave forming might be the most efficient way to provide wideband holograms. If the leaky-wave holograms are operable at frequencies other than the preliminary design frequency, the main beam starts to scan the elevation angle [23]. This scannability provided by reflector-enabled leaky wave metasurfaces makes them a suitable choice for frequency-dependent scanning systems.

In this work, we combine the concept of nonforward-surface-wave redirection for ideal wave leakage and the holographic theorem. We propose a parabolic surface-wave reflector for perfect nonforward-mode suppression. The idea of a parabolic perfect electric conductor (PEC) reflecting boundary located next to the cylindrical surface wave launcher makes the redirection of a 2D Bessel formed surface wave to an almost one-dimensional (1D) forward surface wave possible. With this technique, all the energy generated by the cylindrical wave launcher is manipulated to participate in the beamforming process as the forward leaky mode. The theory of holography is applicable to the new design only for the modified surface wave on the metasurface in the presence of a parabolic reflector. Therefore, the resultant all-forward surface wave provides a wide operating frequency bandwidth of 13–18 GHz. Consequent scannability of the elevation angle is obtained. The absence of nonforward modes in the surface wave exciting the holographic surface impedance allows the wave leakage focus on object-wave generation more accurately than a conventional hologram. A directivity greater than 22 dB is obtained for the reflector-enabled hologram over the operating frequency. The antenna radiation scans the elevation angle from 33° to 69° .

II. HOLOGRAPHY PRINCIPLE

When a surface is illuminated by two electromagnetic waves, they may interact with each other differently depending on the capture point. The interaction produced is due to the reinforcing or canceling at various positions on the surface [24]. The holography principle is based on recording the intensity resulting from the interference

process. The theory says that by exciting the recorded interference with one of the waves participating in the interference production, the other one will be constructed. The reference wave ψ_{ref} excites the recorded interference to construct the object wave ψ_{obj} . The reference and object waves often stand for the incident wave and the wave scattered from the modulated surface, respectively. However, in our application, the reference wave is a surface wave traveling on the modulated surface and the object wave is made by leakage through the path on which the reference wave moves. The resultant intensity of the interaction between the two waves is [25]

$$I = |\psi_{\text{ref}} + \psi_{\text{obj}}|^2. \quad (1)$$

After some simplification, the intensity is

$$I = |\psi_{\text{ref}}|^2 + |\psi_{\text{obj}}|^2 + 2|\psi_{\text{ref}}||\psi_{\text{obj}}|\cos(\phi_{\text{ref}} - \phi_{\text{obj}}), \quad (2)$$

ϕ indicates the wave phase value. We use the surface-impedance parameter as the recorded interference of two interacting waves. However, there may be other options regarding the wavelength. To represent the interference in the form of surface impedance, Eq. (2) can be rewritten as

$$Z_s = jX_0[1 + M \times \text{Re}(\psi_{\text{ref}}\psi_{\text{obj}}^*)], \quad (3)$$

where X_0 and M are the average surface impedance and the modulation factor, respectively. To illustrate the definitions of the parameters, consider a sinusoidally modulated surface impedance (which is the case in holographic modulation). X_0 represents the surface impedance constant value about which the modulation is performed and M is the modulation factor and specifies the magnitude of sinusoidal variations about X_0 . Figure 1 shows a schematic representation of X_0 and M for a 1D sinusoidally modulated surface impedance.

A monopole surface-wave launcher is suitable for exciting the surface impedance on a conventional center-fed hologram. The monopole radiates like a long conducting wire on the metasurface ($z = 0$). A long conducting wire carrying current $\mathbf{I} = I_0\hat{\mathbf{z}}$ radiates a TM wave propagating in the radial direction. For metasurface applications, we often are interested in the TM_0 mode. The electric and magnetic

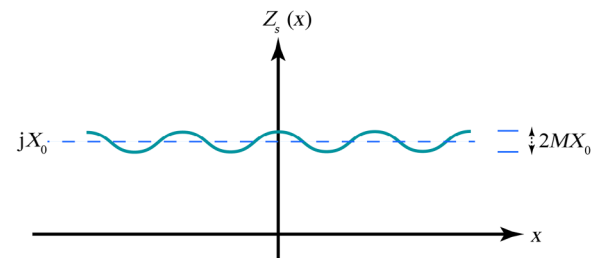


FIG. 1. X_0 and M for a 1D modulated surface impedance.

fields produced by a cylindrical-surface-wave launcher for an isotropic surface impedance are [22]

$$H_\phi = -J_{\text{sw}} H_1^{(2)}(k_{\text{sw}}\rho), \quad (4)$$

$$E_\rho = Z_s J_{\text{sw}} H_1^{(2)}(k_{\text{sw}}\rho). \quad (5)$$

Therefore, the reference wave form can be treated as $H_1^{(2)}(k_{\text{sw}}\rho)$. The large-argument asymptotic form of the reference wave is

$$\begin{aligned} H_1^{(2)}(k_{\text{sw}}\rho) &\approx \sqrt{\frac{2}{\pi k_{\text{sw}}\rho}} e^{-j[(\beta_{\text{sw}} - j\alpha_{\text{sw}})\rho - 3\pi/4]} \\ &= \left(\sqrt{\frac{2}{\pi k_{\text{sw}}\rho}} e^{-\alpha_{\text{sw}}\rho + j3\pi/4} \right) e^{-j\beta_{\text{sw}}\rho}. \end{aligned} \quad (6)$$

Rewriting $H_1^{(2)}(k_{\text{sw}}\rho)$, we obtain

$$H_1^{(2)}(k_{\text{sw}}\rho) \approx \left(a_0 \sqrt{\frac{2}{\pi \sqrt{\beta_{\text{sw}}^2 + \alpha_{\text{sw}}^2} \rho}} e^{-\alpha_{\text{sw}}\rho} \right) e^{-j\beta_{\text{sw}}\rho}, \quad (7)$$

where $k_{\text{sw}} = \beta_{\text{sw}} - j\alpha_{\text{sw}}$ and a_0 is a complex constant. The surface impedance in Eq. (3) requires the interactive waves to be normalized. Finally, the reference wave can be written as [5]

$$\psi_{\text{ref}} = e^{-j\beta_{\text{sw}}\rho}. \quad (8)$$

For surface-wave propagation on a surface ($z = 0$ plane) with complex surface impedance, the unmodulated normalized surface impedance with respect to the free-space impedance $\sqrt{\mu/\epsilon}$ is $Z_s = R_0 + jX_0$. For a TM radial wave above this surface, the magnetic field can be written as

$$H_\phi = A_0 H_1^{(2)}(k_{\text{sw}}\rho) e^{-jk_z z}, \quad (9)$$

and the wave number is

$$k^2 = k_z^2 + k_{\text{sw}}^2. \quad (10)$$

The E_ρ component for a TM wave can be derived with use of Maxwell's equation,

$$j\omega\epsilon E_\rho = -\frac{\partial H_\phi}{\partial z}, \quad (11)$$

and the E_ρ component is

$$E_\rho = \frac{A_0 k_z}{\omega\epsilon} H_1^{(2)}(k_{\text{sw}}\rho) e^{-jk_z z}. \quad (12)$$

To obtain the wave impedance, the ratio of two transverse electric and magnetic field components is needed:

$$Z_1 = \frac{E_\rho}{H_\phi} = \frac{-k_z}{\omega\epsilon} = \frac{-k_z}{k} \sqrt{\frac{\mu}{\epsilon}}. \quad (13)$$

By equating the normalized surface impedance and wave impedance at $z = 0$

$$Z_s = \frac{Z_1}{\sqrt{\frac{\mu}{\epsilon}}} = -\frac{k_z}{k}, \quad (14)$$

$$k_z = kZ_s = kR_0 + jkX_0.$$

Substituting k_z in Eq. (10), we obtain

$$\begin{aligned} k_{\text{sw}} = \beta_{\text{sw}} - j\alpha_{\text{sw}} &= \sqrt{k^2 - (kR_0 + jkX_0)^2} \\ &= k\sqrt{1 + X_0^2 - R_0^2 - 2jX_0R_0}. \end{aligned} \quad (15)$$

When the medium is designed to be loss-free and if we ignore radiation from the surface, R_0 can be set to zero ($X_0 \gg R_0$). The approximation $R_0 \approx 0$ can be applied, and Eq. (15) simplifies to [26]

$$\beta_{\text{sw}} \approx k\sqrt{1 + X_0^2}. \quad (16)$$

This approximation is derived for a surface with constant reactive value. However, this is also valid for a loosely modulated surface impedance [small values of M in Eq. (3)] [27]. Since we are seeking to generate an object wave propagating in θ_0 and ϕ_0 spherical angle directions, we define the object-wave wave vector as

$$\mathbf{k} = k \sin \theta_0 \cos \phi_0 \hat{\mathbf{x}} + k \sin \theta_0 \sin \phi_0 \hat{\mathbf{y}} + k \cos \theta_0 \hat{\mathbf{z}}, \quad (17)$$

and the position vector as

$$\mathbf{r} = x\hat{\mathbf{x}} + y\hat{\mathbf{y}} + z\hat{\mathbf{z}}. \quad (18)$$

Therefore, the object-wave expression in the desired direction is

$$\psi_{\text{obj}} = e^{-j\mathbf{k}\cdot\mathbf{r}} = e^{-j(kx \sin \theta_0 \cos \phi_0 + ky \sin \theta_0 \sin \phi_0 + kz \cos \theta_0)}. \quad (19)$$

The surface-impedance pattern on the $z = 0$ plane in this case is

$$\begin{aligned} Z_s = jX_0 \left[1 + M \sin \left(\beta_{\text{sw}}\rho - kx \sin \theta_0 \cos \phi_0 \right. \right. \\ \left. \left. - ky \sin \theta_0 \sin \phi_0 - \psi_0 + \frac{\pi}{2} \right) \right], \end{aligned} \quad (20)$$

where ψ_0 is the phase of a_0 in Eq. (7). The electric aperture field just above the interactive surface impedance is [22]

$$\mathbf{E}_{\text{apr}} = \hat{\rho} E_{\rho 0} e^{-j(kx \sin \theta_0 \cos \phi_0 + ky \sin \theta_0 \sin \phi_0)} e^{-j(\psi_0 - \frac{\pi}{2})} \times \sqrt{\frac{2}{\pi \sqrt{\beta_{\text{sw}}^2 + \alpha_{\text{sw}}^2} \rho'}} e^{-j\beta_{\text{sw}} \rho'} e^{-\alpha_{\text{sw}} \rho'}. \quad (21)$$

The amplitude $E_{\rho 0}$ and phase ψ_0 are specified by the source parameters. Primed letters are used to avoid misconception in the following analysis. The electric aperture field is obtained in a way that the attenuation constant α_{sw} represents the wave leakage. For a radiative aperture, the far-zone electric field is [28]

$$\mathbf{E}_{\text{far}}(r, \theta, \phi) \approx \frac{jk}{2\pi r} e^{-jkr} (f_{\theta} \hat{\theta} + f_{\phi} \hat{\phi}), \quad (22)$$

$$f_{\theta}(\theta, \phi) = f_x \cos \phi + f_y \sin \phi,$$

$$f_{\phi}(\theta, \phi) = \cos \theta (-f_x \sin \phi + f_y \cos \phi),$$

$$f_x = \int_0^a \int_0^{2\pi} (\mathbf{E}_{\text{apr}} \cdot \hat{\mathbf{x}}) e^{jk(x' \sin \theta \cos \phi + y' \sin \theta \sin \phi)} \rho' d\phi' d\rho', \quad (23)$$

$$f_y = \int_0^a \int_0^{2\pi} (\mathbf{E}_{\text{apr}} \cdot \hat{\mathbf{y}}) e^{jk(x' \sin \theta \cos \phi + y' \sin \theta \sin \phi)} \rho' d\phi' d\rho'. \quad (24)$$

Here we explore the electric field in the object-wave direction θ_0 and ϕ_0 . To fulfill this aim, derivations of $f_{\theta}(\theta_0, \phi_0)$ and $f_{\phi}(\theta_0, \phi_0)$ are necessary. Substituting \mathbf{E}_{apr} in Eqs. (23) and (24), we obtain

$$f_{\theta}(\theta_0, \phi_0) = \int_0^a \int_0^{2\pi} E_{\rho 0} e^{-j\psi_0} \sqrt{\frac{2}{\pi \sqrt{\beta_{\text{sw}}^2 + \alpha_{\text{sw}}^2} \rho'}} \times e^{-\alpha_{\text{sw}} \rho'} \cos(\phi' - \phi_0) \rho' d\phi' d\rho', \quad (25)$$

$$f_{\phi}(\theta_0, \phi_0) = \int_0^a \int_0^{2\pi} E_{\rho 0} e^{-j\psi_0} \sqrt{\frac{2}{\pi \sqrt{\beta_{\text{sw}}^2 + \alpha_{\text{sw}}^2} \rho'}} \times e^{-\alpha_{\text{sw}} \rho'} \sin(\phi' - \phi_0) \rho' d\phi' d\rho'. \quad (26)$$

The integrations above lead to zero, meaning that the electric field vanishes at θ_0 and ϕ_0 , which was the direction expected to propagate the object wave. Figure 2 shows the distributed pattern for a symmetric conventional center-fed hologram. The antenna is designed to radiate at 18 GHz at $\theta_0 = 45^\circ$ and $\phi_0 = -90^\circ$. As is obvious, the holographic

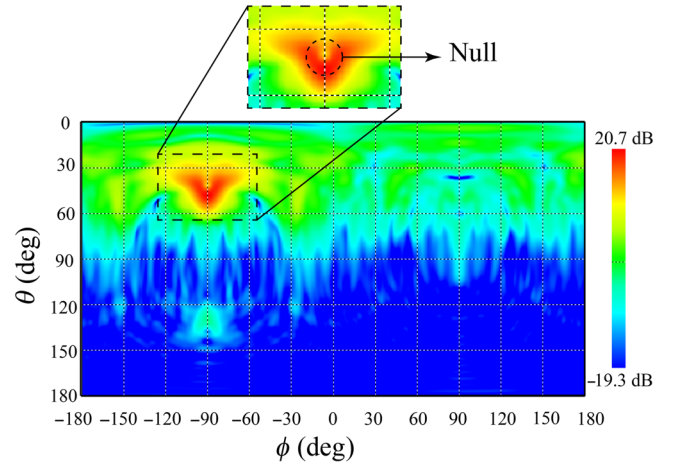


FIG. 2. The distributed 2D radiation pattern of the high-resolution conventional radiative hologram illustrating the undesired null in the object-wave direction in the far-zone electric field pattern.

theorem is unable to predict the null in the design direction for a high-resolution realized hologram at the design frequency. Notice that the analytic calculations predict a pure null in the object-wave direction when the surface impedance is realized with infinite resolution. Therefore, the ideal analytic condition is not achievable. However, in Fig. 2 a simulation with sufficient resolution is shown to clarify the destructive effect of a null on the radiation pattern. This figure indicates that the electric field magnitude is at least 10 dB (10 times) smaller than the neighboring area in the pattern. The structure is designed on the basis of the procedure introduced in Refs. [5,29] using hexagonal unit cells to realize the surface impedance. The integrations (25) and (26) are valid for a practical structure in the case that the discretization resolution is high enough, otherwise the null in the design direction may disappear [23]. Also, for holograms that avoid use of a center-fed surface-wave launcher, the null disappears due to the disruption of surface-wave distribution symmetry. Another way to remove the null is to form a compensating phase correction by enforcing manual phase discontinuity on the surface-impedance distribution [30,31]. All the suggestions offered to improve hologram operation are only for a narrow frequency band in the vicinity of the design frequency.

The holographic leaky-wave radiators are extremely restricted by frequency variation. Holographic antennas are often designed to generate an object wave at a single frequency. However, a practical advantage of leaky-wave radiators is the scannability over a frequency range. A physical interpretation of the limited operating frequency of holograms is a destructive effect called the “rabbit’s ears phenomenon” [19]. On a 1D x -directed leaky-wave radiator fed with a surface-wave launcher producing $\psi_{\text{ref}} = e^{-j\beta|x|}$ with sinusoidal modulation aimed to radiate

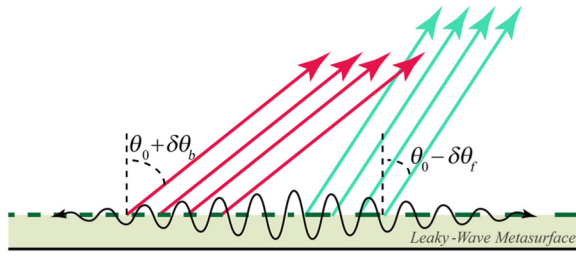


FIG. 3. Comparison of leaky waves from forward and backward surface waves on a 1D metasurface.

in a tilted direction θ_0 , the periodicity of the surface impedance is different in forward and backward regions of the surface impedance. While the forward region is modulated to let the surface wave leak at θ_0 , the backward region should be designed for beamforming at $90^\circ + \theta_0$. Then the surface impedance in the backward region needs to be modulated with lower periodicity than in the forward region. The situation is ideal for operation at design frequency f_0 . However, the wave-leakage directions for each of the forward-region generated and backward-region generated waves show different propagation directions when the surface-wave launcher starts to operate at a frequency slightly lower than f_0 . For a launcher operating at $f_0 - \delta f$, the forward and backward leaky waves propagate at $\theta_0 - \delta\theta_f$ and $\theta_0 + \delta\theta_b$, respectively (as illustrated in Fig. 3). By alteration of the frequency to values other than f_0 , the surface wave fronts on two sides of the wave launcher face surface-impedance steps forcing the surface waves on each side to leak in different directions. The resulting beams that deviate from each other are like rabbit's ears and the phenomenon is named after them [19]. This destructive effect of nonforward leaky waves at frequencies other than the design frequency on the total radiated object wave can be generalized to 2D leaky-wave metasurfaces. Metasurfaces using a monopole wave launcher support cylindrical-surface-wave fronts propagating along the ρ direction. In Fig. 4, for a holographic metasurface aimed to produce a tilted object wave, a picture of the object-wave propagation path is projected on the metasurface. The projected picture on the metasurface is the path along

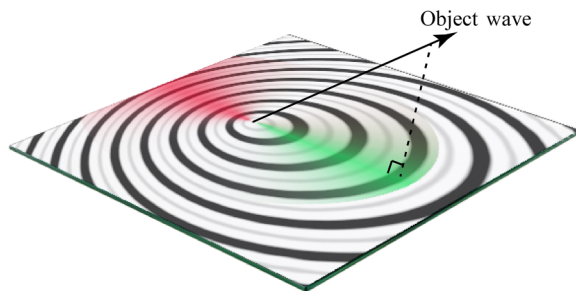


FIG. 4. Forward and backward surface leaky waves for a 2D hologram supporting cylindrical-surface-wave excitation.

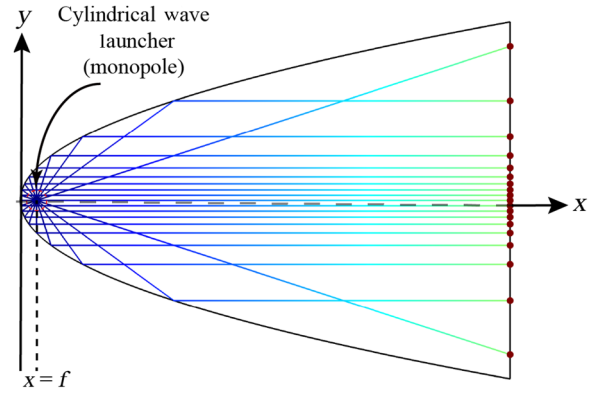


FIG. 5. The scattered rays leaving a monopole radiator located at the focal point of a parabolic PEC boundary.

which the ideal forward surface leaky wave is traveling on the waveguiding metasurface (shown in green on the metasurface in Fig. 4). Considering the cylindrical excitation on the metasurface, as we move in the azimuth direction away from the green path and monitor the effect of the radial surface wave on the object-wave radiation pattern, the destructive effect of the rabbit's ears phenomenon increases by getting away from the green path until the worst case occurs for the all-backward surface-leaky-wave path shown in red. Therefore, any nonforward surface leaky wave has a destructive effect on the bandwidth of the radiator. Conventional holograms use a cylindrical wave launcher and leaky-wave metasurfaces designed to operate in a microwave regime, and the presence of nonforward surface leaky waves is the reason for their very narrow operating frequency.

A parabolic reflector illuminated by a cylindrical wave launcher placed at the focal point of a parabola is a geometry that collimates incoming waves to parallel waves propagating in a single direction. The concept can be used to overcome the rabbit's ears phenomenon in leaky-wave holograms. With regard to Fig. 5, half of the radiated waves in the $x < f$ region are redirected into the forward surface-leaky-wave direction and rest of the waves leaving the monopole radiator in the $x > f$ region also change their propagation path as they are reflected from the parabolic reflector. Thus, almost all of the surface leaky waves are collimated into ideal forward surface leaky waves. It is important to notice that the power of the nonforward surface leaky waves is not eliminated; we are converting what was thought to be destructive for radiation characteristics of radiative holograms into the ideal form of surface leaky waves.

III. METASURFACE DESIGN

We introduce a reflector-enabled holographic metasurface. Placing a reflector next to the cylindrical-surface-wave launcher can break the symmetry of the surface-wave

configuration and results in a null-free pattern at the design frequency f_0 . On the other hand, by choosing the reflector profile to be a parabolic surface-wave reflector with a cylindrical-surface-wave launcher at the focal point (f) of the parabola, we can treat the whole metasurface as a bundle of 1D leaky-wave radiators that provide considerable scannability due to the perfect redirection of almost all nonforward surface waves. Therefore, highly reduced beam width and improved directivity over a wide frequency range are predicted in comparison with conventional holographic antennas. The preliminary holographic reference wave (5) can be assumed when the parabolic reflector is not located on the structure. After embedding of the parabolic reflector next to the surface-wave launcher, the holographic reference wave is modified. The parabolic PEC boundary follows the equation

$$x = \frac{1}{4f}y^2. \quad (27)$$

Figure 5 provides an insight into the holographic-reference-wave configuration after the placement of the parabolic reflector on the hologram using ray optics. The cylindrical rays leaving the monopole surface-wave launcher are collimated into an x -directed bundle of rays [28]. These secondary reflected rays are all in phase after passing the $x = f$ vertical line. Therefore, if we ignore the wave function in the small area between the $x = 0$ and $x = f$ lines, the reference wave in the other areas of the 2D hologram can be assumed to be planar in-phase surface waves. For the sake of higher accuracy in reference-wave estimation, the simulation results are used to form the surface impedance with use of COMSOL MULTIPHYSICS [32].

Knowing the reference and object waves leads to a 2D distribution of the surface impedance (Z_s) with use of Eq. (3). Once the surface impedance is derived, the theory for wave reconstruction is applied. The resulting 2D surface-impedance distribution in the presence of a parabolic reflector is shown in Fig. 6. The theoretical holographic surface impedance needs to be realized to be practically capable of beamforming. To realize this surface impedance, an isotropic lattice and patch must be used.

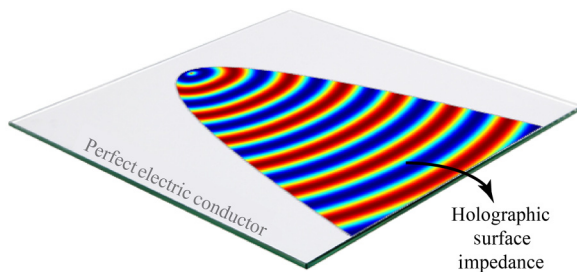


FIG. 6. Two-dimensional distribution of the surface impedance on a parabolic-reflector-enabled hologram.

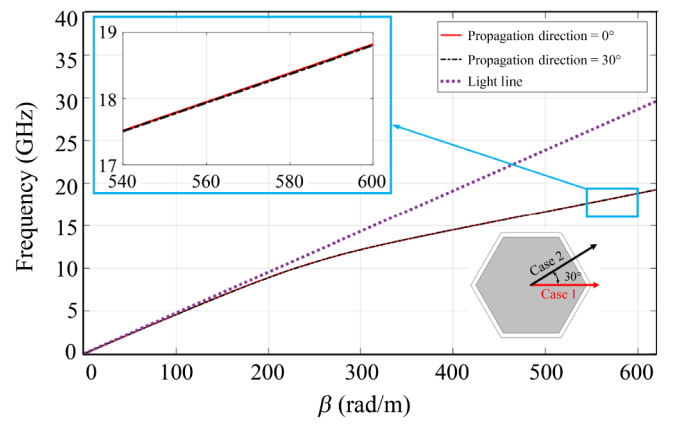


FIG. 7. Dispersion curve of the hexagonal unit cell (lattice and patch) for two different propagation directions.

The isotropy of the surface impedance is dependent on the lattice type and patch geometry. A hexagonal lattice and patch are used to realize the surface impedance for the holograms.

The simulation results in Fig. 7 indicate that the dispersion curves for different propagation directions on a hexagonal unit cell are unchanged in the vicinity of our frequency of interest. These propagation directions are chosen to be the most different cases that can be supported on the hexagonal unit cell.

The patch sizes needed for realization of the surface impedance are shown in Fig. 8. For our application, the total hexagonal-unit-cell side length is chosen to be 1.7 mm and the dielectric substrate relative permittivity is 3.55, with a thickness of 1.524 mm. The modulation factor M in Eq. (3) determines the depth of the sinusoidal space-dependent variations around the average surface impedance and it controls the attenuation constant α . For low values of M , the surface wave obtains enough travel length on the surface and gradual wave leaking with proper accuracy. In contrast, for high values for M , consequent larger sinusoidal variations on the modulated surface make

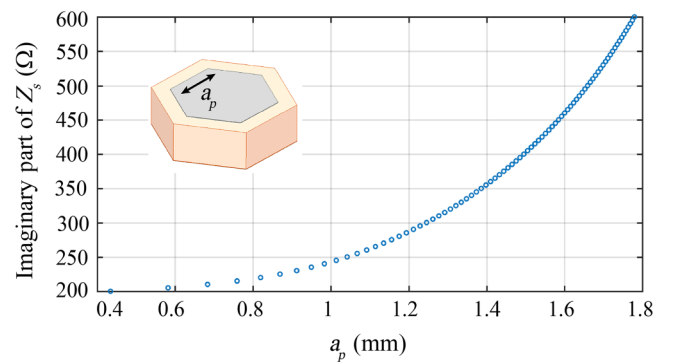


FIG. 8. Imaginary surface impedance as a function of patch side length (a_p).

the surface wave leave the surface in a short length. Therefore, the leaking procedure does not have enough space and time to form the object wave with desired accuracy. High side-lobe levels are observed in this case. However, our choosing very small values for M reduces the attenuation constant along the travel path, and object-wave construction requires a long travel path. Therefore, there is a trade-off between the object-wave accuracy and practical waveguiding path length. We chose $M = 0.35$ for our application. Since the parabolic-reflector-enabled leaky-wave metasurface collimates the surface wave, the surface leaky wave can be treated as an array of unidirectional forward surface leaky waves. The radiation directivity for such a structure is [16]

$$D \propto \frac{\beta_{\perp(-1)}}{\alpha_{\parallel(-1)}} = \frac{\sqrt{\omega^2 \mu_0 \epsilon_0 - [\kappa + 2\pi(-1)/d]^2}}{\alpha_{\parallel(-1)}}, \quad (28)$$

where κ is the fundamental harmonic of parallel-propagation parameters, including the fundamental phase constant $\beta_{\parallel(0)}$ and attenuation constant $\alpha_{\parallel(0)}$ ($\kappa = \beta_{\parallel(0)} - j\alpha_{\parallel(0)}$), d is the period of the modulated surface impedance, $\beta_{\perp(-1)}$ is the phase constant of the leaky wave, and $\alpha_{\parallel(-1)}$ is the attenuation constant of the wave in the waveguiding metasurface. As the modulation factor M increases, the surface wave tends to radiate sooner while traveling on the metasurface and the attenuation constant $\alpha_{\parallel(-1)}$ increases, which results in a lower directivity value and object-wave accuracy. Therefore, higher side-lobe levels are expected while the antenna scans the elevation angle.

Discretization of 2D surface impedance into subdomains each assigned to a certain surface impedance is needed for practical realization. Figure 9 shows the design procedure for the proposed hologram with a parabolic reflector. First, the surface-impedance distribution is obtained with the holographic theorem. Then, a 2D spatial distribution of hexagonal-patch side lengths a_p is plotted using the curve in Fig. 8. Finally, a fully synthesized hologram using hexagonal patches can be realized by our sampling from the a_p spatial distribution. The hexagonal patches with different sizes show different values of surface impedance. Therefore, the whole discretized 2D surface-impedance distribution can be synthesized with use of the corresponding hexagonal patch for each subdomain.

To illustrate the concept, some radiation characteristics of the conventional and the proposed parabolic-reflector-enabled holographic metasurface radiators both fed by cylindrical-surface-wave launchers are compared. The object-wave direction and design frequency are assumed to be $\theta_0 = 70^\circ$ and $f_0 = 18$ GHz for both holograms. This selection of θ_0 provides scanning property by frequency decrease. To compare the effect of nonforward surface

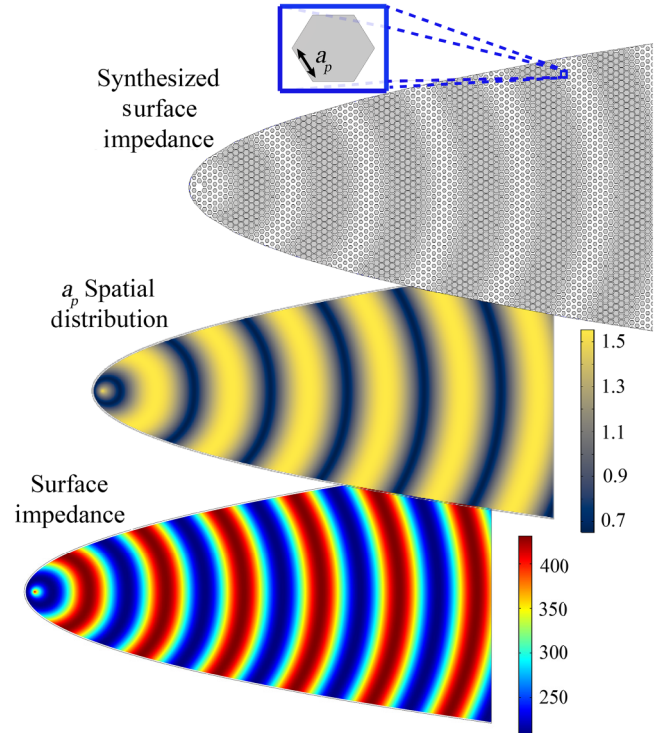


FIG. 9. Design procedure for the proposed hologram. The surface impedance is obtained from holography and the spatial distribution of hexagonal patches of required dimensions a_p (mm) related to the corresponding surface impedance. The hologram fully synthesized from hexagonal patches is shown at the top.

leaky waves on the hologram operating bandwidth, the distributed 2D radiation patterns at $f = 17$ GHz are shown in Fig. 10. Both holograms use hexagonal unit cells to realize the surface impedance. Figure 10(a) shows the radiation pattern of the conventional hologram. The theoretical calculations in Sec. II suggest that the null exists only in the pattern at f_0 . However, if we alter the frequency from $f_0 - \delta f$ to f_0 , the electric field magnitude vanishes in the object-wave direction (ϕ_0 and θ_0) continuously and there might be a spot in the pattern where the value is lower in comparison with the neighboring area at 17 GHz. It must be noted that the rabbit's ears phenomenon is the dominant destructive effect in the radiation pattern at any frequency except f_0 . The rabbit's ears phenomenon ruins the radiation pattern and any other destructive effects (like a null) are difficult to distinguish and somewhat negligible.

As is clear in Fig. 10, the significant destructive effect of nonforward surface leaky waves on the object wave makes the radiation pattern unacceptable for the conventional hologram. In contrast, the hologram obtained with a parabolic reflector by redirection of the nonforward surface leaky waves into forward ones has a main-lobe magnitude of 22.9 dB at $f = 17$ GHz, while the conventional hologram reaches 15.3 dB. Figure 11 illustrates how the proposed hologram maintains highly directive over 13–18 GHz.

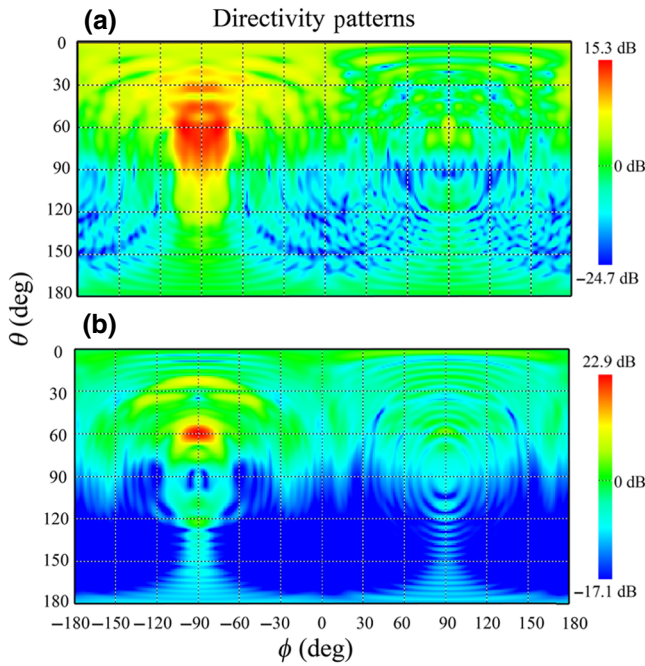


FIG. 10. Comparison of simulated [33] 2D patterns of conventional (a) and parabolic-reflector-enabled (b) holographic radiators at $f_0 - \delta f$ (17 GHz).

By lowering of the operating frequency, the hologram tends to scan the θ angle, and $\theta_{\text{scan}} = 60.0^\circ$ is obtained for $f = 17$ GHz.

IV. EXPERIMENTAL RESULTS

A holographic surface impedance calculated for object-wave generation at θ_0 scans the elevation angles by frequency variation. After surface-impedance realization, the 2D surface-impedance distribution remains unchanged for all reference-wave frequencies. When the monopole-radiator frequency is set to a value lower than f_0 , the realized surface impedance corresponds to an object wave propagating along a direction nearer to the normal axis to the metasurface plane (lower value of elevation angle θ_0).

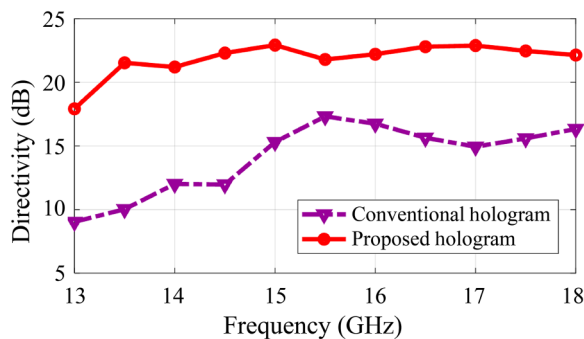


FIG. 11. Full-wave simulation of the conventional and proposed holograms with respect to frequency.

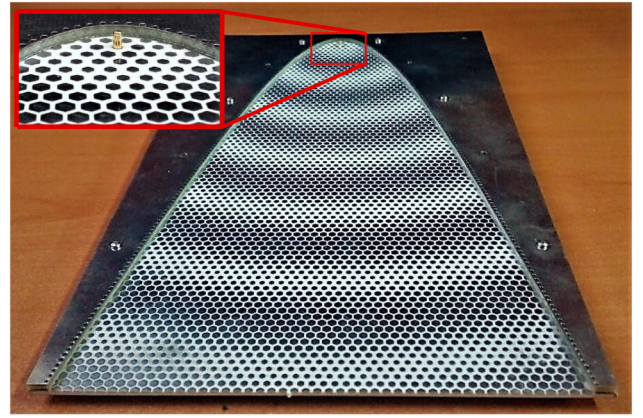


FIG. 12. Fabricated prototype of the proposed holographic metasurface aimed at generating a tilted object wave.

This is also true when the monopole-radiator frequency is set to frequencies higher than f_0 and the elevation angle is larger than θ_0 . Therefore, a major facility provided by wideband holographic metasurfaces is elevation-angle scanning. The wideband holographic metasurface with the parabolic reflector needs to be realized with hexagonal unit cells. Figure 12 shows the fabricated prototype of the parabolic-reflector-enabled hologram. The structure includes two layers: the waveguiding metasurface and the surface-wave reflector. The metasurface is realized with hexagonal unit cells and the parabolic reflector is realized by metalized via holes mimicking the role of the PEC boundary condition. When periodic vias with a period smaller than twice the diameter of the vias are used as the PEC reflector, the band gap prevents the incoming waves from penetrating from the vias in the microwave regime [34]. For further verification, reflection from an array of metalized via holes (1-mm diameter and 1-mm spacing at $f_0 = 18$ GHz) and a metal bulk are compared in Fig. 13, showing simulation results for the 2D distribution of the electric field generated by a cylindrical wave launcher next

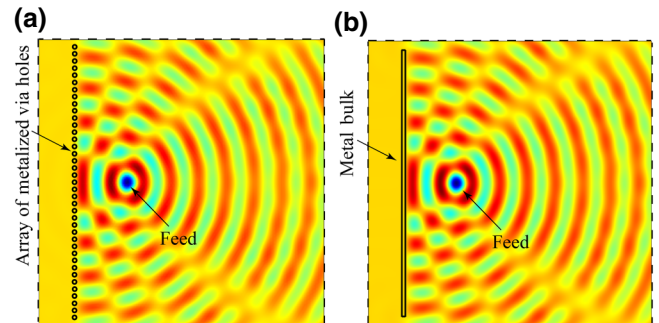


FIG. 13. Simulation results for reflection from an array of metalized via holes (a) and metal bulk (b) next to a cylindrical wave launcher. The surrounding boundary condition is reflectionless (dashed lines) for both cases.

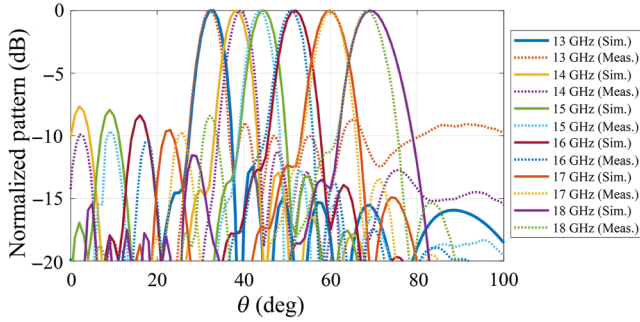


FIG. 14. Simulation (solid lines) and measurement (dashed lines) results for normalized directivity of the parabolic-reflector-enabled holographic antenna.

to both vias and metal bulk. The results indicate that the vias can almost perfectly act as a PEC boundary condition.

Experimentally, use of metal bulk as a reflector is not recommended for integrated structures. Metal bulks make the structure heavy and costly, and metalcasting is needed. In contrast, the use of metalized via holes embedded in dielectric sheets (e.g., FR-4 and RO4003) can lower the fabrication demands and cost. Since the wave is coupled to the surface, a PEC reflecting boundary with finite height suffices for the desired reflection conditions. However, ideal results may be obtained when the reflector height is infinitely extended. Considering the practical conditions, the reflector height is chosen as 1.6 mm. The radiation-pattern results for the simulation and measurement over a frequency range of 13–18 GHz are shown in Fig. 14. The simulation and measurement results have good agreement, indicating the wideband elevation-angle scanning from 33° to 69° . This enables a good scanning application in microwave tracking and communication systems instead of large phased-array antennas.

The fabricated prototype is tested in an anechoic chamber as a receiving antenna and with a double-ridged horn as the transmitting antenna.

V. CONCLUSION

In this paper, we explore the holographic theorem for leaky-wave metasurfaces using surface-wave reflectors. Leaky-wave holographic metasurfaces can be implemented for beamforming in a specific direction. If a surface-wave reflector is placed on a holographic surface, reference-wave modification is necessary. Therefore, the holographic surface-impedance distribution is modified depending on the reflector geometry. Full-wave calculation of the surface impedance in the presence of the reflector can overcome the restriction to closed-form 2D scattered fields known for certain reflector geometries and any arbitrary-shaped reflector profile can be chosen to be placed on a radiative hologram. Also, full-wave calculation has priority over any approximation of the surface impedance.

The conventional center-fed holographic antennas are not capable of beamforming in the object-wave direction when the surface impedance is realized with high accuracy and resolution. It is shown analytically there is a null in the radiation pattern of the high-resolution conventional holograms at the design frequency. Breaking of the reference-wave symmetry with respect to the origin removes the null from the radiation pattern at the design frequency f_0 . Also, a wise selection of the reflector geometry can rearrange the surface leaky waves and result in a wide operating-frequency bandwidth. The overall structure properties and selection of the surface-wave-reflector-profile geometry require various considerations:

(a) The rabbit’s ears phenomenon for 2D holograms suggests that the nonforward modes are the reason for the restricted operating-frequency bandwidth of conventional center-fed holograms.

(b) Any approach to modify nonforward modes, such as elimination, absorption, and redirection of these modes, can lead to a wide operating bandwidth of leaky-wave holograms.

(c) Redirecting surface waves may seem to have priority over elimination and absorption because all the power generated by the monopole can participate in the reference wave and no energy loss occurs.

(d) A parabolic surface-wave reflector can be a perfect choice for the reflector profile. The incoming waves from the focal point of a parabola are converted to parallel in-phase forward modes after reflection from the parabolic PEC boundary condition.

(e) Cylindrical surface leaky waves need to be instantly redirected into parallel waves, otherwise nonforward modes will still have a destructive effect on the pattern and scannability as they travel toward the parabolic reflector before redirection. Hence, the distance between the wave launcher (focal point) and parabolic reflector should be chosen small enough, such a fraction of the wavelength (5 mm for our experimental setup).

A parabolic surface-wave reflector can redirect a nonforward surface wave and provide considerable operating bandwidth. On the other hand, because of surface-wave confinement resulting from reflector embedding on the metasurface, the diffraction effect of 1D leaky-wave structures is suppressed and a better side-lobe level is obtained. In addition, in some applications, because of the lack of space or other reasons, the presence of a reflector on the radiative surface is inevitable. The antenna using the parabolic reflector is enabled for frequency scanning, which is confirmed by simulation and measurement. The directivity at different frequencies within the operating bandwidth of the proposed antenna is highly improved compared with the conventional hologram.

-
- [1] D. R. Smith, J. B. Pendry, and M. C. K. Wiltshire, Metamaterials and negative refractive index, *Science* **305**, 788 (2004).
- [2] N. Engheta and R. W. Ziolkowski, *Metamaterials: Physics and Engineering Explorations* (John Wiley and Sons, Piscataway, NJ, 2006).
- [3] N. Yu, P. Genevet, M. A. Kats, F. Aieta, J. P. Tetienne, F. Capasso, and Z. Gaburro, Light propagation with phase discontinuities: Generalized laws of reflection and refraction, *Science* **334**, 333 (2011).
- [4] A. Oliner and A. Hessel, Guided waves on sinusoidally modulated reactance surfaces, *IRE Trans. Antennas Propag.* **7**, 201 (1959).
- [5] B. H. Fong, J. S. Colburn, J. J. Ottusch, J. L. Visher, and D. F. Sievenpiper, Scalar and tensor holographic artificial impedance surfaces, *IEEE Trans. Antennas Propag.* **58**, 3212 (2010).
- [6] W. Fuscaldo, D. Comite, A. Boesso, P. Baccarelli, P. Burghignoli, and A. Galli, Focusing Leaky Waves: A Class of Electromagnetic Localized Waves with Complex Spectra, *Phys. Rev. Appl.* **9**, 054005 (2018).
- [7] H. Liu and K. J. Webb, Leaky wave radiation from planar anisotropic metamaterial slabs, *Phys. Rev. B* **81**, 201404(R) (2010).
- [8] Z. H. Jiang, Q. Wu, and D. H. Werner, Demonstration of enhanced broadband unidirectional electromagnetic radiation enabled by a subwavelength profile leaky anisotropic zero-index metamaterial coating, *Phys. Rev. B* **86**, 125131 (2012).
- [9] S. N. Tsvetkova, D.-H. Kwon, A. Daz-Rubio, and S. A. Tretyakov, Near-perfect conversion of a propagating plane wave into a surface wave using metasurfaces, *Phys. Rev. B* **97**, 115447 (2018).
- [10] D.-H. Kwon, Lossless tensor surface electromagnetic cloaking for large objects in free space, *Phys. Rev. B* **98**, 125137 (2018).
- [11] N. Marcuvitz, On field representations in terms of leaky modes or eigenmodes, *IRE Trans. Antennas Propag.* **4**, 192 (1956).
- [12] A. C. Tasolamprou, T. Koschny, M. Kafesaki, and C. M. Soukoulis, Near-infrared and optical beam steering and frequency splitting in air-holes-in-silicon inverse photonic crystals, *ACS Photon.* **4**, 2782 (2017).
- [13] F. Monticone and A. Alu, Bound states within the radiation continuum in diffraction gratings and the role of leaky modes, *New J. Phys.* **19**, 093011 (2017).
- [14] D. Gabor, A new microscopic principle, *Nature* **161**, 777 (1948).
- [15] P. F. Checcacci, V. Russo, and A. M. Scheggi, Holographic antennas, *Proc. IEEE* **56**, 2165 (1968).
- [16] R. E. Collin and F. J. Zucker, *Antenna Theory* (McGraw-Hill, New York, 1969).
- [17] J. H. Choi and T. Itoh, in: *Handbook of Antenna Technologies*, edited by Z. Chen (Springer, Singapore, 2015).
- [18] F. Monticone and A. Alu, Leaky-wave theory, techniques, and applications: From microwaves to visible frequencies, *Proc. IEEE* **103**, 793 (2015).
- [19] Y. B. Li, X. Wan, B. G. Cai, Q. Cheng, and T. J. Cui, Frequency-controls of electromagnetic multi-beam scanning by metasurfaces, *Sci. Rep.* **4**, 6921 (2014).
- [20] M. Nannetti, F. Caminita, and S. Maci, in *2007 IEEE Antennas and Propagation Society International Symposium* (IEEE, Honolulu, HI, USA, 2007), p. 5813.
- [21] G. Minatti, F. Caminita, E. Martini, M. Sabbadini, and S. Maci, Synthesis of modulated-metasurface antennas with amplitude, phase, and polarization control, *IEEE Trans. Antennas Propag.* **64**, 3907 (2016).
- [22] G. Minatti, M. Faenzi, E. Martini, F. Caminita, P. De Vita, D. Gonzalez-Ovejero, M. Sabbadini, and S. Maci, Modulated metasurface antennas for space: Synthesis, analysis and realizations, *IEEE Trans. Antennas Propag.* **63**, 1288 (2015).
- [23] M. M. Moeini, H. Oraizi, and A. Amini, in *2018 48th European Microwave Conference (EuMC)* (IEEE, Madrid, 2018), p. 428.
- [24] P. Hariharan, *Optical Holography: Principles, Techniques and Applications* (Cambridge University Press, Madrid, 1996).
- [25] P. Hariharan, *Basics of Interferometry* (Elsevier, Amsterdam, 2010).
- [26] R. E. Collin, *Field Theory of Guided Waves* (Wiley-IEEE Press, New York, 1991), 2nd ed.
- [27] A. M. Patel and A. Grbic, A printed leaky-wave antenna based on a sinusoidally-modulated reactance surface, *IEEE Trans. Antennas Propag.* **59**, 2087 (2011).
- [28] R. S. Elliot, *Antenna Theory and Design* (Wiley-IEEE Press, Hoboken, NJ, 2003).
- [29] M. Li, S. Xiao, and D. F. Sievenpiper, Polarization-insensitive holographic surfaces with broadside radiation, *IEEE Trans. Antennas Propag.* **64**, 5272 (2016).
- [30] M. Casaletti, M. Smierzchalski, M. Ettorre, R. Sauleau, and N. Capet, Polarized beams using scalar metasurfaces, *IEEE Trans. Antennas Propag.* **64**, 3391 (2016).
- [31] S. Pandi, C. A. Balanis, and C. R. Birtcher, Design of scalar impedance holographic metasurfaces for antenna beam formation with desired polarization, *IEEE Trans. Antennas Propag.* **63**, 3016 (2015).
- [32] COMSOL Multiphysics, <https://www.comsol.com/>.
- [33] CST Studio Suite, Computer Simulation Technology ag, <https://www.cst.com/>.
- [34] F. Xu and K. Wu, Guided-wave and leakage characteristics of substrate integrated waveguide, *IEEE Trans. Microw. Theory Tech.* **53**, 66 (2005).